Int. J. Heat Mass Transfer. Vol. 31, No. 10, pp. 2175–2189, 1988
Printed in Great Britain

0017–9310/88 $3.00 + 0.00

Mixed convection friction factors and Nusselt numbers in vertical annular and subchannel geometries

VICTOR IANNELLO,† KUNE Y. SUH‡ and NEIL E. TODREAS
Department of Nuclear Engineering, Massachusetts Institute of Technology, 77 Massachusetts Avenue, Cambridge, MA 02139, U.S.A.

(*Received* 24 *June* 1987 *and in final form* 24 *March* 1988)

Abstract—Analytical solutions are obtained for fully developed vertical laminar mixed convection flows within annular and conventional rod bundle subchannel geometries. Friction factors and Nusselt numbers are presented and fitted as functions of Gr_q/Re. A modified friction factor is defined to be used in applications where only bulk-averaged fluid temperatures are available, as in the case of lumped parameter analyses and most one-dimensional experiments. It is shown that the modified friction factor can vary significantly from the standard definition, which highlights the necessity of using the modified friction factor in analyses where the bulk density is used to calculate the gravity component of the axial pressure gradient. Finally, the present analysis is compared with experimental data available in the literature.

1. INTRODUCTION

MIXED convection (also referred to as combined free and forced convection) in vertical channels occurs in fluid systems when the externally imposed axial pressure gradient is sufficiently low to make local buoyancy effects nonnegligible. These flows can be encountered in many types of heat exchange equipment where the potential exists for a high power-to-flow ratio, including nuclear reactors, heat exchangers, and passive solar systems.

A number of workers have determined the laminar fully developed velocity profile of mixed convection flow in a vertical circular tube [1–5]. Hallman [6] obtained extensive heat transfer data for water in a heated vertical tube for both upflow and downflow in the developing and fully developed regimes. Kemeny and Somers [7] also obtained heat transfer data in a heated vertical tube using water and oil as the test fluids. In addition, they obtained pressure drop data which indicated that as the power-to-flow ratio increased, the frictional loss increased. They accounted for this increase by defining a mixed convection friction factor ratio, f/f_o, which increased with Gr_q/Re. The ratio f/f_o represents the ratio of mixed convection to forced convection friction factors taken at the same Reynolds number. Bishop *et al.* [8] obtained an analytical expression for f/f_o for fully developed laminar mixed convection flow in a circular tube for heated upflow. Heated downflow, however, was not included.

Sherwin [9] has similarly presented an analysis of fully developed laminar mixed convection flow through an annular duct with its inner radius heated. Velocity profiles, temperature profiles, and Nusselt numbers were presented for an outer radius to inner radius ratio of three. The limiting Nusselt number obtained as Gr_q/Re approached zero was consistent with the forced convection result of Lundberg *et al.* [10] for this radius ratio. Sherwin also obtained heat transfer data for downflow [9] in the heated annulus which, however, did not match the trends of the analysis due to buoyancy-induced turbulence. Maitra and Raju [11] extended Sherwin's analysis to higher Gr_q/Re, although the validity of their analytical result is questionable since, for the range investigated, flow reversal in some regions of the channel is predicted which violates the assumptions of the original analysis. They do, however, present data for heated upflow through an annular channel, and the data do follow the analysis trend of an increase in the Nusselt number as heating is increased. An analytical prediction of the friction factor ratio was not made.

Several workers have investigated the buoyancy effects on fully developed laminar flow through infinite rod bundle geometries [12–15]. Kim and Wolf [16] predicted mixed convection subchannel friction factors and Nusselt numbers for finite rod bundles with heated upflow. Wang *et al.* [17] investigated the buoyancy effect on subchannel friction factors and Nusselt numbers for finite rod arrays of triangular and square shape for both heated upflow and heated downflow. The mixed convection friction factors presented, though, were not computed directly from the calculated velocity profile, but rather from a quantity that is dependent on the choice of reference temperature (or density) in the channel. Efthimiadis and

† Current address: Creare, Inc., Etna Road, Hanover, NH 03755, U.S.A.
‡ Current address: Fauske and Associates, Inc., 16W070 West 83rd Street, Burr Ridge, IL 60521, U.S.A.

NOMENCLATURE

A_f cross-sectional flow area
$\mathrm{ber_o}\,\xi, \mathrm{bei_o}\,\xi$ $J_o(i^{3/2}\xi) = I_o(i^{1/2}\xi) = \mathrm{ber_o}\,\xi + i\,\mathrm{bei_o}\,\xi$
$\mathrm{bei'_o}\,\xi$ $\mathrm{d(bei_o}\,\xi)/\mathrm{d}\xi$
$\mathrm{ber'_o}\,\xi$ $\mathrm{d(ber_o}\,\xi)/\mathrm{d}\xi$
c_p coolant specific heat at constant pressure
D rod outside diameter
D_e equivalent hydraulic diameter
f Darcy–Weisbach friction factor
F modification parameter for friction factor, $\pm(2Gr_q/Re)T_b/f\,Re$
g gravitational acceleration
Gr_q Grashof number, $\rho_o^2\beta g D_e^4\bar{q}''/k\mu^2$
$Gr_{q,D}$ $(D/D_e)^4 Gr_q$
Gz Graetz number, $Re\,Pr/(z/D_e)$
H wire wrap lead length
i $\sqrt{-1}$
I_o modified Bessel function of first kind of order 0
J_o Bessel function of first kind of order 0
k thermal conductivity
K_o modified Bessel function of second kind of order 0
$\mathrm{ker_o}\,\xi, \mathrm{kei_o}\,\xi$ $Y_o(i^{3/2}\xi) = K_o(i^{1/2}\xi) = \mathrm{ker_o}\,\xi + i\,\mathrm{kei_o}\,\xi$
$\dot{m}$ mass flow rate
n outward normal
N dimensionless outward normal, n/D_e
Nu Nusselt number, $[\bar{q}''/(\bar{t}_w - t_b)](D_e/k)$
p pressure
$[-\mathrm{d}p/\mathrm{d}z]$ pressure gradient
$\hat{p}$ $p + \rho_o g z$
P dimensionless pressure, $\hat{p}/\rho_o u_o^2$
P_h heated perimeter
P_w wetted perimeter
Pr Prandtl number, $c_p\mu/k$
P/D pitch to diameter ratio
q heat input rate
$\bar{q}''$ average heat flux, $q/P_h L$
Q dimensionless heat flux, $-k\nabla t/\bar{q}'' = q''/\bar{q}''$
r radial coordinate
r_i inner radius
r_o outer radius or distance to zero shear stress plane
r_w duct wall distance
R dimensionless radial coordinate, r/D_e
Ra_H Rayleigh number, $(Gr_q/Re)/4$
Re Reynolds number, $\rho_o u_o D_e/\mu$
R_i r_i/D_e
R_o r_o/D_e
R_w r_w/D_e
s denominator in the angle of symmetry, π/s
t temperature
T dimensionless temperature, $(t - t_o)k/\bar{q}''D_e$
u axial velocity
U dimensionless axial velocity, u/u_o
w gap distance
$2w/D$ gap to diameter ratio
z axial coordinate
Z dimensionless axial coordinate, z/D_e.

Greek symbols
α inner-to-outer radius ratio of annulus, r_i/r_o
β thermal expansion coefficient, $(1/\rho)(-\partial\rho/\partial T)_p$
η $(4(Gr_q/Re)(P_h/P_w))^{1/4}$
μ dynamic viscosity
ϕ colatitudinal (or 'cone') angle
ρ fluid density
θ azimuthal (or 'polar') angle
τ_w wall shear stress
ξ variable.

Subscripts
b bulk averaged
f frictional
FC forced convection (equation (39))
i inner
MC mixed convection (equation (39))
o equivalent isothermal, reference, outer or zeroth order
w wall.

Todreas [18] obtained mixed convection pressure drop and heat transfer data from bare and wire-wrapped bundles with P/D ratio equal to 1.25. The Nusselt numbers measured for the wire-wrapped bundle matched Wang *et al.*'s analysis [17] for the range of Gr_q/Re values considered.

This review of the literature for fully developed laminar mixed convection flow illustrates that while the circular tube has been extensively studied, other geometries of interest have not. For example, Nusselt number results exist only for the inner radius heated annulus [9], and for heated upflow and heated downflow in subchannels of finite triangular and square arrays [17].

An additional problem arises in the evaluation of the gravity term of the momentum equation. In order to properly evaluate this term, the *spatially-averaged* fluid density must be known. Typically, however, the *bulk-averaged* (mixing-cup) fluid properties are measured in experiments and calculated by lumped

parameter analysis codes. For mixed convection flows, the bulk-averaged and spatially-averaged densities may significantly differ, and thus there is an inherent error introduced by using the bulk density to compute the gravity pressure gradient. Alternatively, this error can be eliminated by including a separate correction term in the momentum equation to account for this difference. Instead of correcting both the friction and gravity pressure gradient terms for mixed convection effects, the gravity correction term is included in the friction term. In doing so, a modified friction factor is defined which includes the gravity pressure gradient correction term. This modified friction factor can then be used in combination with the bulk density to calculate the total (gravity plus friction) pressure gradient in a channel without error.

This work was performed to obtain standard and modified friction factor and Nusselt number results under fully developed laminar mixed convection conditions for a variety of azimuthally symmetric and subchannel geometries under aiding and opposing flow conditions for which solutions do not presently exist. In providing these results, general solutions to the conservation equations are obtained in non-dimensional form. These can then be used to obtain solutions for other geometries not considered here as the need arises. The Nusselt number results are compared with applicable experimental data.

The tabular and graphical results for all geometries investigated in this work are available in ref. [26].

2. GENERAL NON-DIMENSIONAL SOLUTION OF THE CONSERVATION EQUATIONS

2.1. *Velocity profile*

It is desired to solve for the fully developed laminar velocity and temperature distributions for fluid flowing in vertical heated ducts in the mixed convection regime with no internal heat generation and no secondary flows (i.e. no θ and r components of velocity). The fluid is heated with a uniform axial heat flux prescribed on one surface of the duct, and the heat flux may vary azimuthally.

In the present analysis only the axial velocity distributions are considered in the r- and θ-directions. While the radial and azimuthal velocities might still exist within the channel due to the azimuthally varying heat flux boundary condition, these secondary flows are neglected since:

(1) the time scale of the secondary flow motion is typically much greater than that of the bulk axial flow so that it should have negligible effect on the axial flow profile;

(2) their neglect leads to conservative upper limit values for both the friction factor and the Nusselt number.

To simplify the analysis, it will be assumed that the fluid specific heat, viscosity, and thermal conductivity do not vary with temperature. Following the Boussinesq approximation, variations of the density will also be ignored except for the gravity body force term of the momentum equation where the density is assumed to be of the form

$$\rho = \rho_o[1-\beta(t-t_o)]. \tag{1}$$

The determination of the reference temperature t_o and reference density ρ_o is presented later.

From the previous assumptions, the momentum and energy conservation equations are

$$0 = -\frac{dp}{dz} \mp \rho_o g[1-\beta(t-t_o)] + \mu\nabla^2 u \tag{2}$$

$$\rho_o c_p u\frac{\partial t}{\partial z} = k\nabla^2 t \tag{3a}$$

where z increases in the direction of flow. In equation (2), the minus sign on the second term on the right-hand side applies to flows in which the buoyancy force is in the same direction as the bulk flow (heated upflow or cooled downflow), a situation called 'aiding flow'. The plus sign applies to flows in which the buoyancy is in the opposite direction to the flow (heated downflow or cooled upflow), a situation called 'opposing flow'.

Now we neglect the axial mass flux gradient, $\partial(\rho u)/\partial z$, by applying the Boussinesq approximation and the fully developed flow condition, and approximate the mass flow rate as $\dot{m} \cong \rho_o u_o A_f$ by neglecting the spatially-averaged product of spatial variations in density and velocity. Then the axial temperature gradient, $\partial t/\partial z$, can be related to the duct wall heat flux through an energy balance as

$$\frac{\partial t}{\partial z} = \frac{\bar{q}'' P_h}{\rho_o u_o A_f c_p}$$

which is substituted into equation (3a), the result being

$$\bar{q}''\frac{P_h}{A_f}\frac{u}{u_o} = k\nabla^2 t. \tag{3b}$$

Equations (2) and (3b) can now be nondimensionalized as

$$0 = -\frac{dP}{dZ}Re \pm \frac{Gr_q}{Re}T + \nabla^{*2}U \tag{4}$$

$$4\frac{P_h}{P_w}U = \nabla^{*2}T. \tag{5}$$

By applying the non-dimensional Laplacian operator ∇^{*2} to equation (4), and utilizing equation (5), T can be eliminated, the result being

$$0 = \pm 4\frac{Gr_q}{Re}\frac{P_h}{P_w}U + \nabla^{*4}U \tag{6}$$

since $(dP/dZ)\,Re$ is a constant term and is eliminated in this process. The general solution (in polar coordinates) to equation (6) can be written as

$$U = \sum_{v=0}^{\infty} \{[a_v \operatorname{ber}_v(\eta R) + b_v \operatorname{bei}_v(\eta R) + c_v \operatorname{ker}_v(\eta R) + d_v \operatorname{kei}_v(\eta R)][e\cos(v\theta) + f\sin(v\theta)]\} \quad (7)$$

for aiding flow, and

$$U = \sum_{v=0}^{\infty} \{[a_v J_v(\eta R) + b_v Y_v(\eta R) + c_v I_v(\eta R) + d_v K_v(\eta R)][e\cos(v\theta) + f\sin(v\theta)]\} \quad (8)$$

for opposing flow, where the parameter η is defined by

$$\eta^4 \equiv 4\frac{Gr_q}{Re}\frac{P_h}{P_w}. \quad (9)$$

For geometries with azimuthal symmetry, equations (7) and (8) reduce to

$$U = a_o \operatorname{ber}_o(\eta R) + b_o \operatorname{bei}_o(\eta R) + c_o \operatorname{ker}_o(\eta R) + d_o \operatorname{kei}_o(\eta R) \quad (10)$$

for aiding flow, and

$$U = a_o J_o(\eta R) + b_o Y_o(\eta R) + c_o I_o(\eta R) + d_o K_o(\eta R) \quad (11)$$

for opposing flow.

For triangular and square arrays, the boundaries $\theta = 0$ and π/s are lines of symmetry where $s = 6$ and 4, respectively. Therefore

$$\left.\frac{\partial U}{\partial \theta}\right|_{\theta=0} = \left.\frac{\partial U}{\partial \theta}\right|_{\theta=\pi/s} = 0. \quad (12)$$

Applying equation (12) to equations (7) and (8) yields $f = 0$ and specifies possible values of v as

$$v = ns, \quad n = 0, 1, 2, \ldots \quad (13)$$

so that equations (7) and (8) can be written as

$$U = \sum_{n=0}^{\infty} \{[a_{ns} \operatorname{ber}_{ns}(\eta R) + b_{ns} \operatorname{bei}_{ns}(\eta R) + c_{ns} \operatorname{ker}_{ns}(\eta R) + d_{ns} \operatorname{kei}_{ns}(\eta R)][\cos(ns\theta)]\} \quad (14)$$

for aiding flow, and

$$U = \sum_{n=0}^{\infty} \{[a_{ns} J_{ns}(\eta R) + b_{ns} Y_{ns}(\eta R) + c_{ns} I_{ns}(\eta R) + d_{ns} K_{ns}(\eta R)][\cos(ns\theta)]\} \quad (15)$$

for opposing flow. The constant e has been incorporated into the constants a_{ns}, b_{ns}, c_{ns} and d_{ns}.

The general solutions for both the azimuthal symmetric geometry and the rod array cases have four sets of constants. These sets of constants are evaluated from the velocity and heat flux boundary conditions. The heat flux at the boundaries is next shown to be a function of $\nabla^{*3}U$. First, a dimensionless heat flux is defined by

$$Q \equiv \frac{q''}{\bar{q}''} = -\frac{k\nabla t}{\bar{q}''} = -\nabla^* T. \quad (16)$$

After applying the ∇^* operator to equation (4) and rearranging, one obtains

$$\pm\frac{\nabla^{*3}U}{Gr_q/Re} = -\nabla^* T. \quad (17)$$

Combining equations (16) and (17) yields

$$Q = \pm\frac{\nabla^{*3}U}{Gr_q/Re}. \quad (18)$$

Equation (18) can be used to relate the heat flux boundary conditions to $\nabla^{*3}U$.

2.2. *Friction factor calculation*

In the last section it was shown that for fully developed conditions the mixed convection velocity profile in the duct is a function of Gr_q/Re, boundary conditions, and geometry. Since the friction factor is directly related to the shear at the fluid–solid interface which results from a velocity gradient normal to the surface, one would expect mixed convection effects to alter the friction factor from the forced convection value. In this section it will be shown how the friction factor is calculated once the velocity profile is known.

A simple force balance shows that

$$\left[-\frac{dp}{dz}\right]_f = \frac{1}{A_f}\int_{P_w} \tau_w \, dP_w \quad (19)$$

where $[-dp/dz]_f$ is the pressure gradient due to skin friction, and τ_w is the fluid shear at the duct wall. For a Newtonian fluid

$$\tau_w = \mu\frac{\partial u}{\partial n} \quad (20)$$

where the normal derivative is defined by

$$\frac{\partial}{\partial n} = \cos\phi\frac{\partial}{\partial r} - \sin\phi\frac{1}{r}\frac{\partial}{\partial \theta} \quad (21)$$

and ϕ is the angle between the surface normal and the θ-direction. (For a radial surface, $\phi = 0$.) After some algebraic manipulation, and introducing the Darcy friction factor, i.e.

$$f \equiv 2\left[-\frac{dp}{dz}\right]_f \frac{D_e}{\rho_o u_o^2} \quad (22)$$

one can solve for $f\,Re$, as

$$f\,Re = \frac{8}{P_w}\int_{P_w}\frac{\partial U}{\partial N} dP_w \quad (23)$$

where the non-dimensional normal derivative is defined by

$$\frac{\partial}{\partial N} \equiv \cos\phi\frac{\partial}{\partial R} - \sin\phi\frac{1}{R}\frac{\partial}{\partial \theta}. \quad (24)$$

For mixed convection flow, we have defined a mixed convection friction factor ratio, f/f_o, where f_o is the forced convection friction factor for the same Reynolds number as for f. For fully developed laminar

flow, $f_o Re$ is a constant, so that the friction factor ratio can be evaluated from

$$(f/f_o) = \frac{f\,Re}{f_o\,Re}. \tag{25}$$

As Gr_q/Re approaches zero, f/f_o approaches one.

2.3. *Temperature profile*

The expressions needed to calculate the mixed convection friction factor were calculated directly from the velocity profile. This is because frictional pressure drop is caused by fluid shear at the wall. Once the velocity profile in the channel is known, one can solve for the temperature field by solving equation (4) for T. The one problem is that the $(-\mathrm{d}P/\mathrm{d}Z)\,Re$ in equation (4) is still an undetermined constant. It will be shown that if the reference temperature is chosen to be the spatially-averaged temperature, the constant $(-\mathrm{d}P/\mathrm{d}Z)\,Re$ can be related to the constant $f\,Re$ already calculated from the velocity profile.

First, $-\mathrm{d}P/\mathrm{d}Z$ as defined is expanded to

$$-\frac{\mathrm{d}P}{\mathrm{d}Z} = \frac{D_e}{\rho_o u_o^2}\left[-\frac{\mathrm{d}p}{\mathrm{d}z} \mp \rho_o g\right]. \tag{26}$$

If ρ_o is assumed to be the spatially-averaged density in the cross-section of the duct, then $\rho_o g$ is the axial pressure gradient due to the gravity body force. The expression in square brackets in equation (26) must therefore represent the axial pressure gradient due to friction, $[-\mathrm{d}p/\mathrm{d}z]_f$, since

$$\left[-\frac{\mathrm{d}p}{\mathrm{d}z}\right] = \pm\left[-\frac{\mathrm{d}p}{\mathrm{d}z}\right]_g + \left[-\frac{\mathrm{d}p}{\mathrm{d}z}\right]_f. \tag{27}$$

Equation (26) can therefore be written as

$$-\frac{\mathrm{d}P}{\mathrm{d}Z} = \frac{D_e}{\rho_o u_o^2}\left[-\frac{\mathrm{d}p}{\mathrm{d}z}\right]_f. \tag{28}$$

Combining equation (22) with equation (28), thereby eliminating $[-\mathrm{d}p/\mathrm{d}z]_f$, results in

$$-\frac{\mathrm{d}P}{\mathrm{d}Z} Re = \frac{f\,Re}{2}. \tag{29}$$

Now that the constant $[-\mathrm{d}P/\mathrm{d}Z]\,Re$ is known, equation (4) can be directly solved for T, resulting in

$$T = \mp \frac{-\dfrac{\mathrm{d}P}{\mathrm{d}Z} Re + \nabla^{*2} U}{Gr_q/Re}. \tag{30}$$

Equation (29) is valid only if ρ_o is calculated at the spatially-averaged temperature defined as

$$t_o \equiv \frac{1}{A_f}\int\int_{A_f} tr\,\mathrm{d}r\,\mathrm{d}\theta. \tag{31}$$

If another reference density and temperature are chosen, equation (29) will give erroneous results. This was the source of error in ref. [17], where an arbitrary reference temperature was chosen.

The bulk-averaged temperature for axial flow is defined as, with $\dot{m}$ taken as $\rho_o u_o A_f$

$$t_b \equiv \frac{1}{\rho_o u_o A_f}\int\int_{A_f} \rho utr\,\mathrm{d}r\,\mathrm{d}\theta \tag{32a}$$

which can be simplified consistent with the Boussinesq approximation of neglecting density variations except for the buoyancy term in the momentum equation to

$$t_b = \frac{1}{u_o A_f}\int\int_{A_f} utr\,\mathrm{d}r\,\mathrm{d}\theta \tag{32b}$$

since $\rho_o \gg \rho - \rho_o$.

Substituting U, T and R for u, t and r, respectively, results in

$$T_b = \frac{D_e^2}{A_f}\int\int_{A_f} UTR\,\mathrm{d}R\,\mathrm{d}\theta. \tag{32c}$$

Once U and T are known, equation (32c) can be integrated numerically. It will be shown that T_b is a necessary parameter for the calculation of the modified friction factor of the next section.

2.4. *Modified friction factor*

To calculate the axial pressure gradient, it is necessary to evaluate the correct pressure gradient due to gravity. Typically, the gravity pressure gradient is calculated assuming the bulk-averaged temperature and density are equal to the spatially-averaged temperature and density, since the bulk temperature can be calculated from lumped parameter analysis without knowledge of the details of the temperature field. As Gr_q/Re increases, the error associated with this approximation also increases.

Specifically, the pressure gradient should be calculated using the spatially-averaged density in equation (27)

$$\left[-\frac{\mathrm{d}p}{\mathrm{d}z}\right] = \pm\rho_o g + \left[-\frac{\mathrm{d}p}{\mathrm{d}z}\right]_f \tag{33}$$

whereas it is usually approximated using the bulk density, i.e.

$$\left[-\frac{\mathrm{d}p}{\mathrm{d}z}\right] \cong \pm\rho_b g + \left[-\frac{\mathrm{d}p}{\mathrm{d}z}\right]_f. \tag{34}$$

Therefore, we seek an easy way to correct for using the bulk density to compute the gravity term in the momentum equation, i.e. to correct the right-hand side of equation (34) to eliminate the approximation. Rather than correcting the gravity term, however, we chose to correct the friction term since the designer will know only the bulk density through his lumped parameter tools, and the correction factor can be readily calculated from previously determined non-dimensional parameters. This leads to the formulation of the correction factor F such that

$$\left[-\frac{dp}{dz}\right] = \pm\rho_b g + \left[-\frac{dp}{dz}\right]_f (1+F). \quad (35)$$

Since equation (33) can be expanded as

$$\left[-\frac{dp}{dz}\right] = \pm\rho_b g \pm (\rho_o - \rho_b) g + \left[-\frac{dp}{dz}\right]_f \quad (36)$$

we see that the factor F is given by

$$F = \pm \frac{(\rho_o - \rho_b) g}{\left[-\frac{dp}{dz}\right]_f}. \quad (37)$$

As can be seen from equation (37), the factor F represents the ratio of the gravity pressure gradient correction to the friction pressure drop, and equals zero for forced convection flows. Substituting equations (1) and (22) into equation (37), the desired expression for F is obtained as

$$F = \pm \frac{\rho_o \beta (t_b - t_o) g}{\frac{f}{D_e}\frac{\rho_o u_o^2}{2}} \equiv \pm \frac{2\frac{Gr_q}{Re} T_b}{f\,Re}. \quad (38)$$

Thus, F can easily be calculated from previously determined non-dimensional parameters.

Hence, the ratio of the mixed to forced convection friction pressure drop which should be used when the axial pressure gradient due to gravity is calculated using the bulk density (as is typically done in lumped parameter codes) is

$$\frac{{}_{MC}[-dp/dz]_f}{{}_{FC}[-dp/dz]_f} = \frac{\frac{f}{D_e}\frac{\rho u_o^2}{2}(1+F)}{\frac{f_o}{D_e}\frac{\rho u_o^2}{2}} = \frac{f}{f_o}(1+F). \quad (39)$$

2.5. *Nusselt number*

Once the temperature distribution is known, the Nusselt number can easily be calculated. By definition

$$Nu \equiv \frac{\bar{q}''}{\bar{t}_w - t_b}\frac{D_e}{k} \quad (40)$$

where $\bar{t}_w$ is the average temperature of the heated surface, which can be calculated from

$$\bar{t}_w = \frac{1}{P_h}\int_{P_h} t r\,d\theta. \quad (41)$$

Equations (40) and (41) can then be nondimensionalized to yield

$$Nu = \frac{1}{\bar{T}_w - T_b} \quad (42)$$

and

$$\bar{T}_w = \frac{D_e}{P_h}\int_{P_h} TR\,d\theta. \quad (43)$$

In geometries where more than one wall is heated, one can use equations (42) and (43) to define a different Nusselt number for each wall. It must be noted, however, that in situations where more than one wall is heated, the Nusselt number obtained for each heated surface will also depend upon the heat fluxes on the other surfaces through T_b. This phenomenon is not unique to mixed convection but occurs also in forced convection.

Now that the generalized conservation equations have been presented, one can proceed to solve the equations for two sets of geometries. For the first set, azimuthal symmetry is assumed, thereby simplifying the analysis. The second geometry set involves subchannels occurring in rod bundle geometries where azimuthal dependencies cannot be ignored.

3. GEOMETRIES WITH AZIMUTHAL SYMMETRY

3.1. *Velocity profile*

Four geometries are investigated in this section. For each geometry, aiding and opposing flow conditions are evaluated. For the first geometry, the duct is assumed to be concentrically annular in shape. The heat flux is imposed at the inner radius and an adiabatic outer radius is assumed. For the second geometry, the duct is annular with an adiabatic inner radius and heat flux imposed at the outer radius. The third geometry is the circular duct, with the heat flux imposed at the wall. The fourth geometry is called the equivalent annulus because, like the annulus, it has an inner and outer radius. The difference is that instead of a no-slip velocity boundary condition being imposed at the outer radius, a zero shear condition is assumed for the equivalent annulus. The equivalent annulus is of interest because it can be used as an approximation to rod array geometries with large spacing, as will be discussed later. For each case, the parameter α is defined as the inner radius to outer radius ratio ($\alpha = 0$ for the circular channel). The solutions for the velocity profiles are obtained by computing a_o, b_o, c_o and d_o from the velocity and heat flux boundary conditions at the inner and outer radii.

Figure 1 shows the aiding flow velocity profile for a typical azimuthally symmetric geometry (inner radius heated annulus). The effect of increasing Gr_q/Re for aiding flow is to redistribute the flow towards the heated wall. Mass continuity requires a corresponding decrease of flow near the adiabatic boundary. For opposing flow, the effect is to redistribute the flow away from the heated wall [26]. There is a corresponding increase of flow near the adiabatic boundary.

3.2. *Friction factor*

In the previous section it was shown that the velocity profile in a duct will be distorted as Gr_q/Re increases. As the velocity profile changes, the fluid shear at the no-slip surfaces must also change, since shear is proportional to the velocity gradient. For aiding flow, the shear will increase at the heated wall

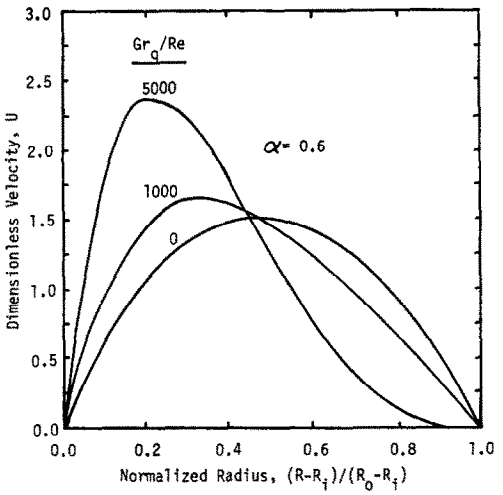

FIG. 1. Velocity profile for the inner radius heated annulus for aiding flow.

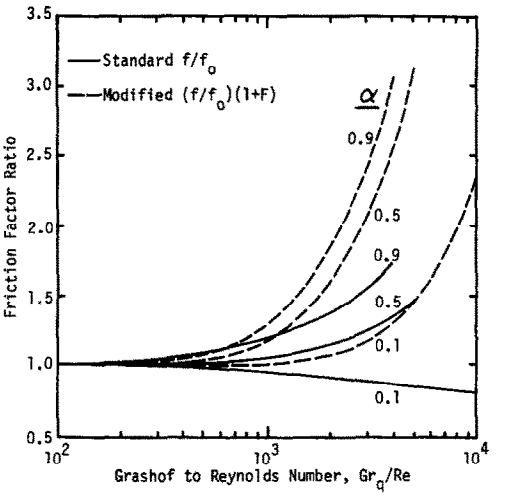

FIG. 2. Standard and modified friction factor ratios for the inner radius heated annulus for aiding flow.

and due to mass conservation, decrease at the adiabatic boundary. For opposing flow, the reverse will occur. These effects cause the friction factor to vary with Gr_q/Re.

The friction factor can be evaluated using the previously derived equations (23) and (24). For geometries with azimuthal symmetry, the surface normal must always be radial so that $\phi = 0$. Equations (23) and (24) can therefore be combined as

$$f\,Re = \frac{8}{P_w}\int_{P_w}\frac{dU}{dR}\,dP_w. \tag{44}$$

The parameter $f_o\,Re$ can be evaluated from the standard results

$$f_o\,Re = \begin{cases} 64 & \text{circle} \\ 64\dfrac{(1-\alpha^2)(1-\alpha)^2}{1-\alpha^4\dfrac{(1-\alpha^2)^2}{\ln\dfrac{1}{\alpha}}} & \text{annulus} \\ 64\dfrac{(1-\alpha^2)^3}{\alpha^2\left(-3+4\alpha^2-\alpha^4+4\ln\dfrac{1}{\alpha}\right)} & \text{equivalent annulus} \end{cases} \tag{45}$$

which can be obtained by solving equation (4) with $Gr_q/Re = 0$, applying the appropriate velocity boundary conditions, and substituting the expression for U into equation (44). The friction factor ratio can then be evaluated from equation (25).

The parameter f/f_o is plotted against Gr_q/Re in Fig. 2 for the inner radius heated annulus. For large α values as the value of Gr_q/Re increases, the velocity distortion increases, producing increased friction factors for aiding flow. For small α the decrease in shear at the adiabatic boundary more than compensates for the increase at the heated surface. As a result, the f/f_o ratio decreases with increasing Gr_q/Re for $\alpha = 0.1$. Corresponding calculations for opposing flow demonstrated a decrease in friction factors with increasing Gr_q/Re for $\alpha = 0.9$ and 0.5 and the inverse behavior for $\alpha = 0.1$ [26].

The friction factor ratio results are fitted to the form

$$\ln(f/f_o) = \sum_{i=0}^{4} g_i\lambda^i \tag{46}$$

where

$$\lambda \equiv \ln(1+Gr_q/Re). \tag{47}$$

The results are presented in Tables 3-2 through 3-7 of ref. [26]. The values of g_i are obtained by least squares error fitting, and less than 5% fitting error results when Gr_q/Re is within the range listed in the table.

3.3. *Modified friction factor*

We can use equations (29) and (30) to solve for the temperature field in the duct once we have obtained an expression for $f\,Re$. Then, equation (32) can be used to find the dimensionless bulk temperature, T_b. For geometries with azimuthal symmetry, equation (32c) simplifies to

$$T_b = 2\pi\frac{D_e^2}{A_f}\int_{R_i}^{R_o} UTR\,dR \tag{48}$$

which can be integrated numerically. Once T_b is obtained, equation (38) is used to solve for F.

Figure 2 shows how the modified friction factor differs from the standard friction factor for the inner radius heated annulus. Corresponding calculations for opposing flow demonstrated a more pronounced difference since the standard friction factor decreased with Gr_q/Re, while the modified friction factor increased with Gr_q/Re for $\alpha = 0.9$ and 0.5 [26].

The above modified friction factor ratio results are fitted to the form

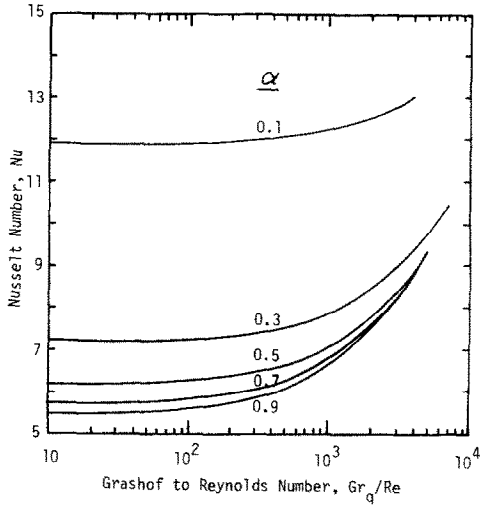

FIG. 3. Mixed convection Nusselt number for the inner radius heated annulus for aiding flow.

$$\ln[(f/f_o)(1+F)] = \sum_{i=0}^{4} g_i \lambda^i \tag{49}$$

as was done for the standard friction factor ratio. The resulting values for g_i are listed in Tables 3-8 through 3-13 of ref. [26].

3.4. *Nusselt number*

The determination of the Nusselt number is trivial once the temperature field is known. The Nusselt number is given directly by equation (42).

Figure 3 shows the Nusselt number vs Gr_q/Re for the inner radius heated annulus. The Nusselt number increases for aiding flow due to increased convection at the diabatic (i.e. heat transfer) wall, and it decreases for opposing flow due to decreased convection at the diabatic wall.

The Nusselt number results are also fitted to the form

$$\ln(Nu) = \sum_{i=0}^{4} g_i \lambda^i \tag{50}$$

as was done for the friction factor ratios. The values of g_i are presented in Tables 3-14 through 3-17 of ref. [26] for the inner radius heated and the outer radius heated annuli, but not for the equivalent annuli which exhibit fairly constant values of the Nusselt number for given α ratios for $Gr_q/Re < 10^4$.

Lundberg *et al.* [10] have solved for the heat transfer in annular geometries for forced convection, hydrodynamically developed, thermally developing flow. Table 1 compares their results for thermally developed flow with the results from the present mixed convection analysis, which were obtained by setting $Gr_q/Re = 0.1$. We see excellent agreement with the forced convection analysis for all values of α reported.

Table 1. Forced convection Nusselt numbers for the annulus

α	Heating location	Aiding	Opposing	Forced convection analysis [10]
0.02	r_i	32.704	32.702	32.70
	r_o	4.734	4.734	4.734
0.05	r_i	17.811	17.811	17.81
	r_o	4.792	4.791	4.791
0.10	r_i	11.906	11.906	11.90
	r_o	4.834	4.834	4.834
0.25	r_i	7.754	7.753	7.753
	r_o	4.905	4.904	4.904
0.50	r_i	6.184	6.181	6.181
	r_o	5.037	5.036	5.036

4. ROD BUNDLE GEOMETRIES

4.1. *Introduction*

The choice of bundle cells is made such that zero shear stress and adiabatic boundary conditions can be applied at inter-cell boundaries. The symmetric segments for a triangular array are shown in Fig. 4.

A problem arises, though, for the edge symmetric segments, since as illustrated in Fig. 4 these are not the geometries conventionally chosen for the noding scheme in the codes such as ENERGY-IV [25] and COBRA. To obtain the friction factors and Nusselt numbers for these subchannel geometries, the symmetric edge segments are broken into three segments with $0 < \theta < \pi/2$, $\pi/2 < \theta < 5\pi/6$, and $5\pi/6 < \theta < \pi$, respectively, for the triangular array, and into two segments with $0 < \theta < \pi/2$ and $\pi/2 < \theta < \pi$, respectively, for the square array. The segments with $0 < \theta < \pi/2$ corresponds exactly to the conventional edge subchannel geometry.

In the interest of brevity, only the friction factor and Nusselt number results for the conventional triangular interior subchannel are presented in this paper for $P/D = 1.25$ and 1.08 to simulate liquid metal reactor fuel and blanket assemblies. Reference [26] contains the results for other subchannels: triangular conventional edge, triangular symmetric edge, square interior, square conventional edge and square symmetric edge.

The application of the mixed convection subchannel friction factors is treated in our subsequent papers relative to reactor core flow redistribution and frictional loss. The difference in flow splits is numerically small. However, the significant consequence of design importance is the bundle frictional pressure drop increase of as much as 85% of the corresponding forced convection value at the bundle $Re = 470$ and $Gr_q/Re = 3500$ under power skew condition, which highlights the importance of utilizing the mixed convection friction factors when the buoyancy plays a dominant role.

Finally, the mathematically predicted flow reversal might not be physically observed due to the buoyancy-induced premature transition to turbulence (in case of liquid) and the intersubchannel crossflow in rod bundles. The application of the proposed correlations should thus be limited to steady, laminar, fully

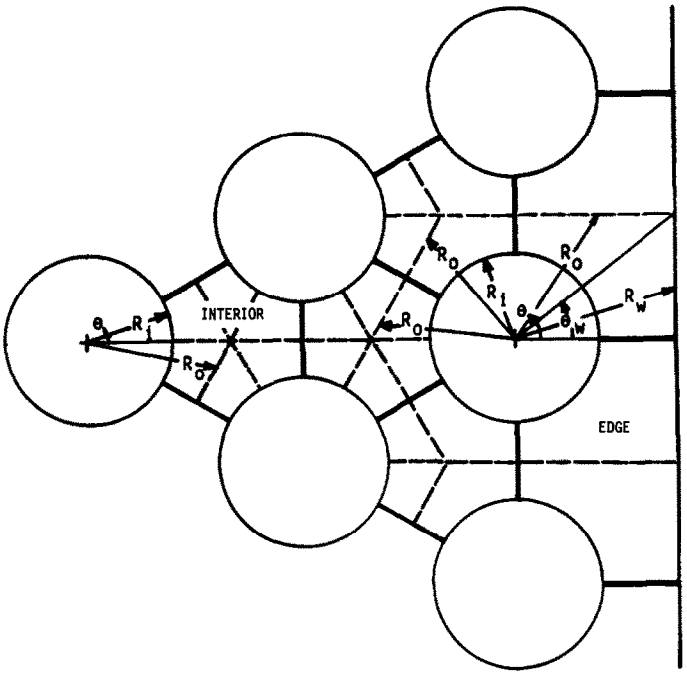

FIG. 4. Symmetric segment (– –) and conventional subchannel (—) geometries for the triangular rod array.

developed, incompressible mixed convective flows with no recirculation.

4.2. *Two-region analysis*

An approach where the boundary conditions apply to only one domain (such as the coolant region) is called a one-region analysis. A more detailed approach would be to assume a uniform or azimuthally varying heat flux along the inner clad surface. For this approach all the fluid region boundary conditions are not explicitly prescribed. Instead, the clad and coolant region boundary conditions are matched at the clad–coolant region interface. This approach is called a two-region analysis. A package of computer programs, originally developed by Kim and Wolf [16], and later modified by Wang *et al.* [17], solves the two-region problem under the assumptions of steady state, thermally and hydrodynamically fully developed laminar flow with no heat generation in the coolant and clad regions. The one-region problem is actually a limiting case of the two-region problem and is obtained when the clad thermal conductivity is much lower than the fluid thermal conductivity so that the heat flux lines remain radial (and thus azimuthally uniform) throughout the clad region. Since the two-region analysis code was available, it was decided to use it with a low clad-to-coolant thermal conductivity ratio, $k_{\text{clad}}/k_{\text{fluid}} = 0.001$, to simulate the one-region analysis with circumferentially uniform heat flux along the clad–coolant interface.

The unknown coefficients in the general solutions for the non-dimensional coolant velocity and temperature, and for the clad temperature, are determined by using the boundary conditions along the zero shear cell boundaries, the clad outside surface, the clad inside surface and, for edge cells, the duct wall inner surface. The boundary conditions can be satisfied continuously at the outside and inside clad surfaces. The imposed conditions along the polygonal cell boundaries and duct wall surface, however, are satisfied by a point-matching technique applied at a prescribed number of points. This leads to a set of linear equations which can be solved by standard methods. Details of the two-region analysis can be found in ref. [17].

4.3. *Velocity profile*

Equations (14) and (15) can be used to obtain the velocity profiles for the interior and edge cells in aiding and opposing flows, respectively. The four sets of coefficients: a_{ns}, b_{ns}, c_{ns} and d_{ns} are computed using the two-region analysis codes [17].

Our subchannel results are presented vs a Grashof number based on the rod outside diameter, D, instead of the equivalent diameter, D_e, noting that the P/D ratio and the equivalent diameter are not independent of each other. The choice of the heated rod diameter as the characteristic length for the Grashof number reflects the existence of the thermally-driven buoyancy effect in heated rod bundle geometries. For other geometries, such as our outer radius heated annulus, although the outside diameter could be used as the characteristic length, we chose to use D_e to be consistent with the literature. The Reynolds number, however, is always based on the equivalent diameter. The two Grashof numbers are related by

$$Gr_q = Gr_{q,D}\left(\frac{D_e}{D}\right)^4. \tag{51}$$

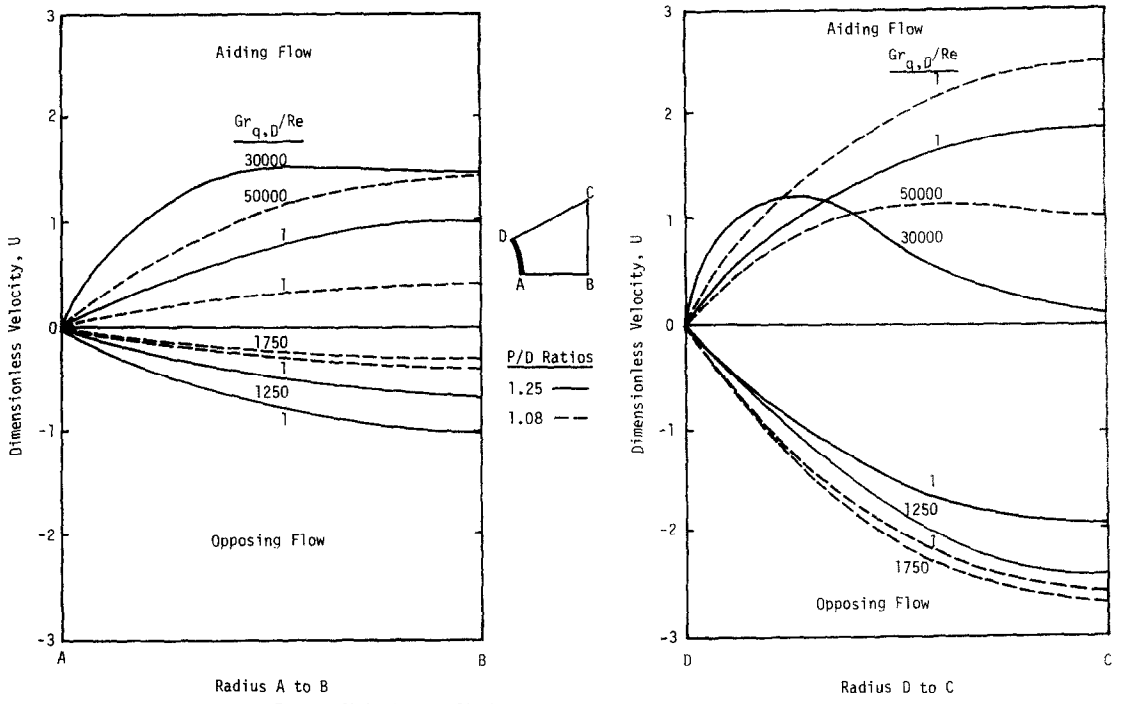

FIG. 5. Velocity profile for the triangular interior subchannel.

Figure 5 shows how increasing $Gr_{q,D}/Re$ distorts the velocity profiles for a typical triangular array interior subchannel. At low $Gr_{q,D}/Re$, the velocity profiles are parabolic and highly nonuniform over the regions within the cell. With increasing $Gr_{q,D}/Re$, we observe that fluid is redistributed within the cell towards the rod surface for aiding flows and away from it for opposing flows. Consequently, the flow becomes more uniform for aiding flows and more nonuniform for opposing flows. These local flow redistribution effects are more predominant in the square array than in the triangular array for the same P/D ratio [26]. Moreover, the local buoyancy effects are more pronounced for $P/D = 1.25$ than for $P/D = 1.08$.

4.4. *Cell-average friction factor*

The friction factor is calculated here using equation (23), which can be rewritten for interior subchannels as

$$f\,Re = 8\frac{\displaystyle\int_0^{\pi/s}\left(\frac{\partial U}{\partial R}\right)_{R_i} R_i\,\mathrm{d}\theta}{\displaystyle\int_0^{\pi/s} R_i\,\mathrm{d}\theta} \tag{52}$$

where $s = 6$ for triangular arrays and $s = 4$ for square arrays. For interior subchannels, the wetted perimeter includes only the outer rod surface, while for edge cells both the rod surface and duct wall must be included.

The $f\,Re$ results for the limiting case of forced convection ($Gr_{q,D}/Re \approx 0.5$) are presented in Table 2 for the triangular array interior subchannels. As shown, the agreement is excellent. The aiding flow predictions are slightly higher than the opposing flow calculations, which is in accord with the heat addition effect of slightly increasing the velocity gradient near the wall for aiding flow and decreasing it for opposing flow.

Table 2. Forced convection $f\,Re$ results for the triangular interior subchannel

	Sparrow and Loeffler	Axford	Rehme	Present analysis			
				Aiding		Opposing	
P/D	[20]	[22]	[22]	Standard	Modified	Standard	Modified
1.05	62.21	61.91	62.32	62.90	62.90	62.82	62.89
1.08	74.21	—	—	74.42	74.42	74.37	74.39
1.10	81.74	81.51	83.24	81.74	81.74	81.52	81.55
1.15	92.35	92.56	92.88	92.64	92.64	92.00	92.04
1.20	99.96	99.80	100.80	99.83	99.83	99.48	99.54
1.25	105.27	105.20	—	105.22	105.22	105.02	105.17
1.50	124.49	124.14	—	124.17	124.14	123.61	124.14
1.80	144.14	—	143.88	144.22	144.00	143.88	143.97
2.00	156.95	157.54	154.20	158.08	157.54	156.95	—
3.00	232.10	233.84	—	244.58	232.70	220.00	—

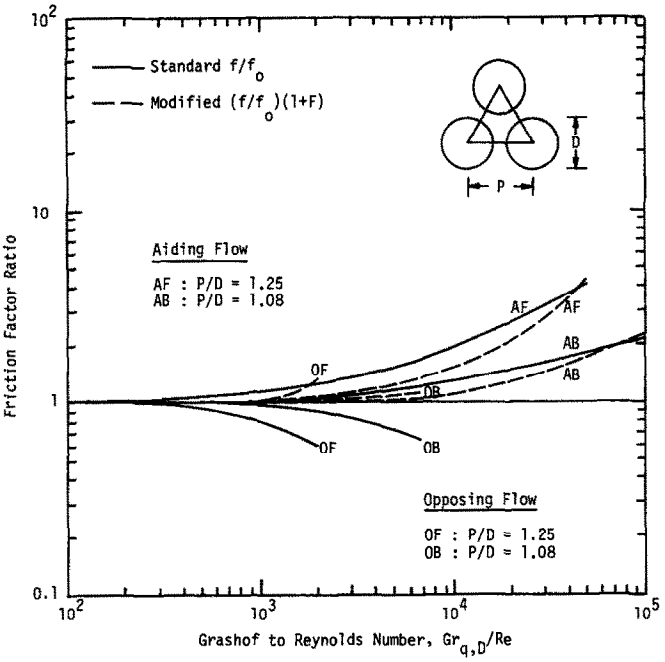

FIG. 6. Standard and modified friction factor ratios for the triangular interior subchannel.

For edge cells, where a segment of interior subchannels is included, the friction factor results are split up such that they can be directly applied to the conventional geometry of the edge subchannel. For the conventional edge subchannels in both triangular and square arrays, the friction factor is defined as

$$f\,Re \equiv 8\left[\frac{\int_0^{\pi/2}\left(\frac{\partial U}{\partial R}\right)_{R_i} R_i\,d\theta}{\int_0^{\pi/2} R_i\,d\theta} + \frac{2}{\pi}\left(\frac{P}{D}\right)\frac{\int_0^{\theta_w}\left[-\left(\frac{\partial U}{\partial N}\right)_{R_w}\right]R_w\,d\theta}{\int_0^{\theta_w} R_w\,d\theta}\right] \quad (53)$$

where $\theta_w = \arctan(P/2w)$, $R_w = w/(D_e\cos\theta)$, and $\partial/\partial N$ at the duct wall is given by equation (24).

Figure 6 shows the friction factors calculated for the triangular array interior subchannel. Tables 4-5 and 4-6 of ref. [26] present the regression coefficients for the fitting equation (46) for standard friction factors with

$$\lambda \equiv \ln(1 + Gr_{q,D}/Re). \quad (54)$$

4.5. *Modified cell-average friction factor*

In order to compute the modified friction factor ratio, $(f/f_o)(1+F)$, one needs to obtain the bulk temperature, T_b. Equation (32c) is used, where the area integrals are performed over the subchannel cross sections. Tables 4-7 and 4-8 of ref. [26] list the regression coefficients for equation (49) with λ given by equation (54) in triangular and square arrays. The results for the typical geometry are also shown in Fig. 6. It is seen that there exist significant differences between the standard and modified friction factors.

Table 3. Forced convection Nusselt numbers for the triangular interior subchannel

P/D	Sparrow *et al.* [21]	Dwyer and Berry [23]	Hsu [24]	Present analysis Aiding	Opposing
1.05	—	1.06	1.06	1.03	1.07
1.08	—	—	—	1.95	1.97
1.10	—	2.94	2.94	2.92	2.93
1.15	—	—	5.14	5.12	5.16
1.20	—	6.90	6.90	6.89	6.90
1.25	—	—	—	8.14	8.13
1.50	—	11.22	11.23	11.23	11.22
1.80	—	13.66	13.67	13.67	14.81
2.00	15.3	15.26	—	15.27	—
3.00	24.0	—	—	24.12	23.98

4.6. *Cell-average Nusselt number*

As with geometries with azimuthal symmetry, the Nusselt number can easily be obtained once the temperature field in the cell is known. Nusselt numbers for the conventional edge subchannel as well as for the symmetric edge segment are reported in ref. [26].

Table 3 presents the limiting forced convection ($Gr_{q,D}/Re \approx 0.5$) Nusselt numbers for the triangular array interior subchannel, which are in good agreement with those in the literature. However, the results of Sparrow *et al.* [21] are for a uniform wall temperature boundary condition. For $P/D \geqslant 2$, though, there is essentially no distinction between the circumferentially uniform wall temperature and uniform

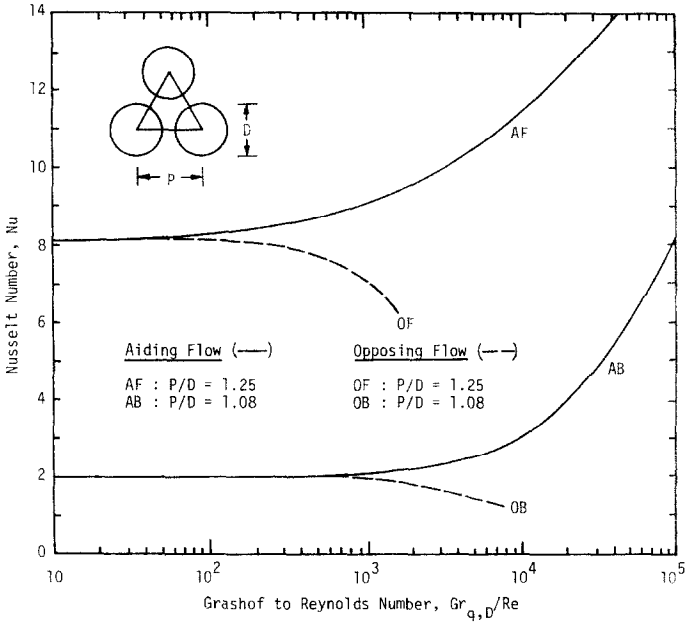

FIG. 7. Mixed convection Nusselt number for the triangular interior subchannel.

heat flux conditions, since the azimuthal variation of either quantity is small. The agreement for $P/D = 2$ and 3 presents appropriate justification for this statement.

Tables 4-10 and 4-11 of ref. [26] list the regression coefficients associated with equation (50) for both triangular and square arrays with λ defined by equation (54). The results for the triangular array interior subchannel are plotted in Fig. 7. In general, the Nusselt number increases for aiding flow due to increased convection at the diabatic wall, and it decreases for opposing flow due to decreased convection at that location.

4.7. *Application of equivalent annulus results to the interior cell geometry*

Sparrow and Loeffler [20] solved for the forced convection friction factors for axial flow in infinite triangular and square rod array geometries. These cases correspond to the interior cell geometries investigated here. They found that as P/D is increased, the effect of neighboring rods is reduced. Normalizing the local shear stress around the rod by the average shear stress and plotting it vs the azimuthal angle θ, they found that, as the P/D ratio increased, the angular dependence of the shear stress decreased. Thus, a subchannel geometry with large P/D ratios could be approximated by a geometry with azimuthal symmetry. This is the basis for choosing the equivalent annulus to describe rod arrays with large P/D ratios. By equating the inner radius of the equivalent annulus model with the rod outer radius for the interior cell in the case of equal flow areas, one finds

$$\alpha = \left[\frac{\pi}{s\tan(\pi/s)}\right]^{0.5}/(P/D). \qquad (55)$$

Table 4. Minimum P/D for equivalent annulus approximation of the interior subchannels

Case	Minimum P/D	Maximum error (%)
Aiding triangular array	1.50	3.15
Aiding square array	3.00	1.02
Opposing triangular array	3.00	1.27
Opposing square array	†	—

† Not recommended.

Since the equivalent annulus friction factor calculation is easier to perform than that for the interior cell, it is desirable to find the range of its applicability. A comparison, from which Table 4 was constructed, was made between the equivalent annulus and the interior cell results, and it illustrates, for the cases considered, the minimum P/D ratios at which the equivalent annulus formulation accurately predicts the interior cell friction factor ratio. It can be seen that the equivalent annulus approximation can be used down to a lower P/D ratio for triangular arrays than for square arrays. The equivalent annulus also approximates aiding flow more closely than opposing flow. For opposing flow in a square array, it is not recommended for any P/D ratio.

5. COMPARISON OF THEORY WITH EXPERIMENTAL DATA

5.1. *Friction factor*

There is a scarcity of mixed convection pressure drop data in the literature as is summarized in the Introduction. Kemeny and Somers [7] measured mixed convection pressure drop for aiding flow in circular tubes using water and oil as the test fluids.

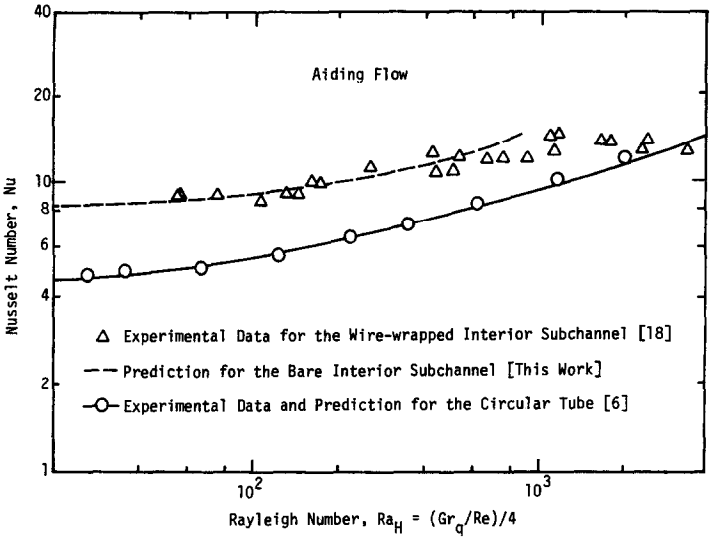

FIG. 8. Experimental data and prediction of the Nusselt number for the MIT 19-rod wire-wrapped bundle.

The friction factor ratio (f/f_o) was plotted against Gr_q/Re, and the data were grouped based on the Graetz number, defined by

$$Gz \equiv (Re\,Pr)/(z/D_e) \tag{56}$$

where z equals zero at the inlet of the pipe. Fully developed flow would thus correspond to a Graetz number approaching zero. Since the velocity field distortion due to buoyancy increases as the flow develops, one would expect the analytical solution for fully developed flow to envelope the experimental data from above. Bishop *et al.* [8] compared these data with mixed convection friction factors for circular tubes in aiding flow. It was found that the analysis enveloped the experimental data from above, which was attributed to flow development effects. Kemeny and Somers used the bulk-averaged temperature (as opposed to the spatially-averaged temperature) to calculate the gravity pressure drop in the tube, and thus the data presented should more correctly be compared with the modified friction factor defined here. When this is done [26], it is found that although the modified friction factor analysis lies closer to the data, there is still sufficient discrepancy to question the validity of attempting to apply the laminar, fully developed flow analysis to these data. Indeed, Kemeny and Somers report that nearly all the data presented lie in the turbulent regime.

5.2. *Nusselt number*

Efthimiadis and Todreas [18] have obtained mixed convection interior cell Nusselt number data from a 19-rod wire-wrapped triangular array bundle with $P/D = 1.25$ and $H/D = 35.2$, where H is the axial helical pitch of the wire. The experimental data are compared to the analytical solution for a bare subchannel with $P/D = 1.25$, along with the circular tube data and prediction of Hallman [6] in Fig. 8. It is seen that our solution adequately predicts the wire-wrapped subchannel data up to a Rayleigh number of about 600, i.e. $(Gr_q/Re)/4 \approx 600$ whereas the circular tube results lie below the subchannel values for $P/D = 1.25$. Also the wire-wrapped subchannel data fall below the bare subchannel prediction starting from Gr_q/Re around 2500, which is presumably due to spacer wire which delays the local buoyancy effect at the heated surface by periodically disturbing the thermal boundary layer at higher ranges of Gr_q/Re. This in turn means that it may not be conservative to apply bare subchannel Nusselt numbers to a wire-wrapped subchannel when $Gr_q/Re > 2500$. For the purpose of comparison between the bare and wire-wrapped subchannels, the Nusselt numbers in Fig. 8 were based on Gr_q/Re rather than on $Gr_{q,D}/Re$ because the equivalent diameters of the two bundles differ for the same P/D ratio.

6. CONCLUSIONS

(1) It has been found that natural convection effects can significantly distort the forced convection isothermal velocity profiles, thereby rendering forced convection analyses inaccurate for the mixed convection flow regime. The fully developed laminar mixed convection friction factors have been consistently evaluated using the buoyancy-affected velocity gradients at the fluid–solid interface for all the channel geometries.

(2) Two types of mixed convection friction factors have been presented in the form of the ratios of their values to the forced convection values as functions of Gr_q/Re or $Gr_{q,D}/Re$, the inner to outer radius ratio for the azimuthally symmetric geometries, and the P/D ratio for the bare rod subchannels. The first type is based on the standard definition of friction factor, f/f_o, which requires that the spatially-averaged fluid density be known if it is to be used in lumped parameter analyses to calculate the axial pressure gradi-

ent. The second type is a modified friction factor, $(f/f_0)(1+F)$, which allows the calculation of the axial pressure gradient based on the bulk mean temperature nominally used in lumped parameter analyses. The behavior of the modified friction factor as a function of Gr_q/Re has been found to considerably differ from that of the standard friction factor particularly for opposing flows in both the annular and subchannel geometries.

(3) Nusselt number results have also been presented as functions of Gr_q/Re or $Gr_{q,D}/Re$ for the annular and subchannel geometries for the condition of circumferentially uniform heat flux at the fluid–solid boundary.

(4) For the rod bundle analysis the cell-averaged friction factors and the Nusselt number have been calculated for the interior and edge channel geometries corresponding exactly to the conventional definition of subchannels. The results can therefore be directly used in a subchannel analysis code. The effect of the duct wall on the edge cells has also been quantitatively estimated.

(5) The standard and modified friction factor ratios and the Nusselt number have been fitted to polynomial equations, i.e. equations (46), (49) and (50), respectively.

Acknowledgement—The authors acknowledge the financial support provided for this work by Power Reactor and Nuclear Fuel Development Corporation of Japan and General Electric Company of the U.S.

REFERENCES

1. G. A. Ostroumov, The mathematical theory of heat transfer in vertical pipes and simultaneous forced and free convection, *Zh. Tekh. Fiz.* **20**(6), 750–757 (1950), in Russian.
2. T. J. Hanratty, E. M. Rosen and R. L. Kabel, Effect of heat transfer on flow field at low Reynolds number in vertical tubes, *Ind. Engng Chem.* **50**(5), 815–820 (1958).
3. T. M. Hallman, Combined forced-and-free laminar heat transfer in vertical tubes with uniform internal heat generation, *Trans. ASME* **78**, 1831–1841 (1956).
4. W. G. Brown, Die Überlagerung von erzwungener und natürlicher Konvektion bei niedrigen Durchsatzen in einem lotrechten Rohr, *VDI ForschHft.* No. 480 (1960).
5. H. L. Greene and G. F. Scheele, Effect of fluid viscosity on combined free forced convection flow phenomena in vertical pipes, *A.I.Ch.E. Jl* **16**(6), 1039–1047 (1970).
6. T. M. Hallman, Experimental study of combined forced and free laminar convection in a vertical tube, NASA TN D-1104 (1961).
7. G. A. Kemeny and E. V. Somers, Combined free and forced-convective flow in vertical circular tubes—experiments with water and oil, *J. Heat Transfer* **84**, 339–346 (1962).
8. A. A. Bishop, J. M. Willis and R. A. Markley, Effect of buoyancy on laminar vertical upward flow friction factors in cylindrical tubes, *Nucl. Engng Des.* **62**, 365–369 (1980).
9. K. Sherwin, Laminar convection in uniformly heated vertical concentric annuli, *Br. Chem. Engng* **13**(11), 1580–1585 (1968).
10. R. E. Lundberg, P. A. McCuen and W. C. Reynolds, Heat transfer in annular passages. Hydrodynamically developed laminar flow with arbitrarily prescribed wall temperatures or heat fluxes, *Int. J. Heat Mass Transfer* **6**, 495–529 (1963).
11. D. Maitra and K. S. Raju, Combined free and forced convection laminar heat transfer in a vertical annulus, *J. Heat Transfer* **97**, 135–137 (1975).
12. M. Iqbal, S. A. Ansari and B. D. Aggarwala, Buoyancy effects on longitudinal laminar flow between vertical cylinders arranged in regular arrays, *Proc. 4th Int. Heat Transfer Conf.*, Vol. 4, NC3.6 (1970).
13. J. W. Yang, Analysis of combined convection heat transfer in infinite rod arrays, *Proc. 6th Int. Heat Transfer Conf.*, Vol. 1, MC-9, pp. 49–54 (1978).
14. J. W. Yang, Buoyancy effects on pressure loss in rod arrays under laminar flow, *ANS Trans.* **32**, 829–830 (1979).
15. J. W. Yang, Heat transfer and fluid flow in regular rod arrays with opposing flow, *Fluid Flow and Heat Transfer Over Rod Bundles*. ASME (1979).
16. J.-Y. Kim, Fully developed mixed convection heat transfer in the finite hexagonal bundles, M.S. Thesis, Nucl. Engng Dept., Massachusetts Institute of Technology (1977); also, J.-Y. Kim and L. Wolf, Laminar mixed convection heat transfer in finite-hexagonal bundles, *ANS Trans.* **27**, 384–385 (1977).
17. S.-F. Wang, N. E. Todreas and W. M. Rohsenow, Subchannel friction factors for bare rod arrays under mixed convection conditions. In *Decay Heat Removal and Natural Convection in Fast Breeder Reactors*, pp. 95–109. Hemisphere, Washington, DC (1981).
18. A. Efthimiadis and N. E. Todreas, Mixed convection and hydrodynamic modeling of flows in rod bundles, Nucl. Engng Dept., Massachusetts Institute of Technology, Report PNC/MIT-11TR (1984).
19. T. Okada, A. Efthimiadis, V. Iannello and N. E. Todreas, Mixed convection pressure drop in vertical rod bundles, *Proc. 3rd Int. Topical Meeting on Reactor Thermal Hydraulics*, Vol. 2, 16.C (1985).
20. E. M. Sparrow and A. L. Loeffler, Jr., Longitudinal laminar flow between cylinders arranged in regular array, *A.I.Ch.E. Jl* **5**(3), 325–330 (1959).
21. E. M. Sparrow, A. L. Loeffler, Jr. and H. A. Hubbard, Heat transfer to longitudinal laminar flow between cylinders, *J. Heat Transfer* **83**, 415–422 (1961).
22. R. K. Shah and A. L. London, *Laminar Flow Forced Convection in Ducts*, Supplement 1 to *Advances in Heat Transfer, 1978*. Academic Press, New York (1978).
23. O. E. Dwyer and H. C. Berry, Laminar-flow heat transfer for in-line flow through unbaffled rod bundles, *Nucl. Sci. Engng* **42**, 81–88 (1970).
24. C.-J. Hsu, Laminar- and slug-flow heat transfer characteristics of fuel rods adjacent to fuel subassembly walls, *Nucl. Sci. Engng* **49**, 398–404 (1972).
25. S.-K. Cheng and N. E. Todreas, Hydrodynamic models and correlations for bare and wire-wrapped hexagonal rod bundles—bundle friction factors, subchannel friction factors and mixing parameters, *Nucl. Engng Des.* **92**(2), 227–251 (1986).
26. V. Iannello, K. Y. Suh and N. E. Todreas, Mixed convection friction factors in flow channels, Nucl. Engng Dept., Massachusetts Institute of Technology, Report PNC/MIT-20TR and GE/MIT-2TR, Rev. 2 (1988).

COEFFICIENT DE FROTTEMENT ET NOMBRE DE NUSSELT DE CONVECTION MIXTE DANS DES GEOMETRIES VERTICALES ANNULAIRES ET DE SOUS-CANAUX

Résumé—Des solutions analytiques sont obtenues pour des écoulements verticaux complètement établis de convection mixte dans des géométries annulaires et des sous-canaux de grappe de barres. Les coefficients de frottement et les nombres de Nusselt sont présentés en fonction du paramètre Gr_q/Re. On définit un coefficient de frottement modifié pour l'utiliser dans des cas où on ne connaît que les températures moyennes du fluide comme dans la plupart des expériences unidimensionnelles. On montre que le coefficient de frottement modifié peut varier sensiblement à partir de la définition standard, ce qui dégage la nécessité d'utiliser le coefficient de frottement modifié dans les analyses où on utilise la masse volumique moyenne pour calculer la composante de gravité dans le gradient axial de pression. Cette étude est comparée aux données expérimentales disponibles dans la bibliographie.

REIBUNGSBEIWERTE UND NUSSELT-ZAHLEN FÜR MISCHKONVEKTION IN VERTIKAL RINGFÖRMIGEN GEOMETRIEN UND AUSSCHNITTEN

Zusammenfassung—Für voll ausgebildete, vertikal laminare Mischkonvektions-Strömungen in ringförmigen Geometrien und Teilausschnitten herkömmlicher Stab-Bündel wurden analytische Lösungen erhalten. Reibungsbeiwerte und Nusselt-Zahlen wurden dargestellt und angepaßt als Funktionen des Parameters Gr_q/Re. Ein modifizierter Reibungsbeiwert wird definiert, der in Anwendungen benutzt werden kann, wo nur über die Masse gemittelte Fluid-Temperaturen verfügbar sind, wie im Fall der Untersuchung verteilter Parameter und der meisten eindimensionalen Experimente. Es wird gezeigt, daß der modifizierte Reibungsbeiwert stark von der Standard-Definition abweichen kann, was die Notwendigkeit der Benutzung des modifizierten Reibungsbeiwerts für Studien herausstellt, bei denen die Massendichte benutzt wird, um die Gravitations-Komponente des axialen Druck-Gradienten zu errechnen. Anschließend wird die vorliegende Untersuchung mit experimentellen Daten aus der Literatur verglichen.

КОЭФФИЦИЕНТЫ ТРЕНИЯ И ЧИСЛА НУССЕЛЬТА ПРИ СМЕШАННОЙ КОНВЕКЦИИ В ВЕРТИКАЛЬНЫХ КОЛЬЦЕВЫХ И ЗАЗОРАХ

Аннотация—Получены аналитические решения для полностью развитых вертикальных ламинарных течений при смешанной конвекции в кольцевых каналах и в зазорах пучка стержней. Коэффициенты трения и числа Нуссельта представлены как функции параметра Gr_q/Re. Предложен модифицированный коэффициент трения для использования в том случае, когда известна усредненная по объему температура жицкости, как например при анализе методом кусочных параметров и в большинстве одномерных экспериментов. Показано, что модифицированный коэффициент трения может значительно отличаться от его стандартного определения, что подчеркивает необходимость использования этого параметра для аналитического исследования в том случае, когда для расчета гравитационной составляющей осевого градиента давления используется объемная плотность. Дано сравнение результатов анализа с имеющимися в литературе экспериментальными данными.